Supplementary Data

Structure and function of the N-terminal domain of the yeast telomerase reverse transcriptase

Petrova, O.A., Mantsyzov, A.B., Rodina, E.V., Efimov, S.V., Hackenberg, C., Hakanpää, J., Klochkov, V.V., Lebedev, A.A., Chugunova, A.A., Malyavko, A.N., Zatsepin, T.S., A.V. Mishin, Zvereva, M.I., Lamzin, V.S., Dontsova, O.A., Polshakov, V.I.

Contents | **Page number**

Experimental details

Cloning, expression and purification of hpTEN mutant variants

Mutations were introduced into the hpTEN expression vector by PCR and self-ligation. PCRs were done with Q5 High-Fidelity polymerase (NEB) according to manufacturer's instructions using the following sets of primers.

TEN mutant variant	Primer pair
N53A/S55A	5'-GCGTACGCTCACGAAGAGCTGATCGATATGC-3' and 5'-AGGCTTTACTAGCGTGGACG-3'
R110A	5'-GCGCTGGTACACACAATCATAGGAACGG-3' and 5'-AAATTCAGGGGACTTCAATAGATTGGTG-3'
E119A	5'-GCGACATTTCTGGATCTCTTGATCAATTACTC-3' and 5'-CGTTCCTATGATTGTGTGTACCAG-3'
W36S	5'-AGCATTGAGCGTGTCAAAGACCGTAA-3' and 5'-TATCTCTCGTCCTGTTCCATGC-3'
R131A/M132A/N134A	5'-GCGGCGGGAGCGGTTTATCTCTGGGGCGAATTGAAC-3' and 5'-CGCCGAGTAATTGATCAAGAGATC-3'

Correctness of all constructed plasmids was verified by sequencing. Subsequent expression of the mutant forms were carried out as described for the wild-type protein. Proper folding of the purified hpTEN mutant variants to the wild-type protein was validated using circular dichroism (CD) spectroscopy (Fig. S19). Circular dichroism measurements were carried out on a Chirascan CD spectrometer (Applied Photophysics) using a 0.01 mm path length. All the CD spectra were recorded at room temperature. A protein concentration of 9 mg/ml was used in 20 mM phosphate buffer, pH 7, 50 mM NaCl for all hpTEM mutant forms.

RNA and DNA synthesis

DNA and RNA oligonucleotides were assembled in an MM-12 synthesizer (Bioautomation) with the phosphoramidite method, according to the manufacturer's recommendations at 25 µmol scale. Protected 2'-deoxynucleotide 3'-phosphoramidites, 2'-TBDMS protected nucleotide 3'-phosphoramidites, Unylinker-CPG (500Å) and S-ethylthio-1H-tetrazole were purchased from ChemGenes. DNAs were cleaved from the support and deprotected using AMA – 1:1 (v/v) concentrated aq. ammonia and 40% aq. methylamine (5 ml) for 3 h at 45°C, the support was washed by water (3×1 ml) and the combined solution was evaporated to dryness. Oligonucleotides were purified by double HPLC. The IE-HPLC purification of oligonucleotides was carried out on a 21×150 mm TSKgel SuperQ-5PW column (13 µm, Tosoh); buffer A: 20 mM Tris-HCl (pH 7.5), 10% acetonitrile; buffer B: 20 mM Tris-HCl (pH 7.5), 1M NaBr, 10% acetonitrile; a gradient of B: 0-5% (1 CV), 5-50% (15 CV); a flow rate of 10 mL/min; temperature 45°C. Fractions were analyzed by LC-MS (Bruker Maxis Impact q-TOF system). Fractions with the full length oligonucleotide (with purity higher than 95%) were pooled and partially evaporated. The RP-HPLC purification of oligonucleotides was carried out on a 21×150 mm Jupiter C18 column (5 µm, Phenomenex); buffer A: 0.05 M triethylammonium acetate (pH 7); buffer B: 0.03 M triethylammonium acetate (pH 7), 80% acetonitrile; a linear gradient of B: 0-100% (8 CV); a flow rate of 5 mL/min; temperature 45°C. Fractions were analyzed by LC-MS (Bruker Maxis Impact q-TOF system). Fractions with the full length oligonucleotide (with purity higher than 95%) were pooled and evaporated. Synthesized single-stranded

oligonucleotides were dissolved in DNAse/RNAse-free water and the amount of material was quantified by UV at 260 nm (Ultraspec 3100, GEHealthcare). The final solutions were frozen at -80°C and oligonucleotides were lyophilized using a FreeZone system (Labconco).

RNAs were cleaved from the support and deprotected using AMA – 1:1 (v/v) concentrated aq. ammonia and 40% aq. methylamine (5 ml) for 1 h at 65°C, support was washed with DMSO (3×2 ml) and the combined solution evaporated to dryness. The gum was dissolved in the mixture of trimethylamine trihydrofluoride (1.5 ml) and DMSO (1 ml) and heated at 60°C for 3.5 h. Crude RNAs were precipitated by the addition of 200 µl of 3 M sodium acetate followed by 10 ml of butanol-1. Solids were separated by centrifugation at 10,000 g and washed thoroughly with ethanol (3×10 ml). Residual ethanol was removed under vacuum and RNAs were purified as described for DNAs.

Sequence and structure alignment

The alignment of the hpTEN, ttTEN, hTEN sequences and their fragments were carried out using GESAMT (1). Automatically generated structure-based sequence alignment was manually adjusted and rendered with *ESPript* (2). DALI search indicated that the structure of hpTEN presented in this manuscript has a Z-score of 7.8 against ttTEN and 3.0 or below against other structures in the PDB. Multiple sequence alignment was performed using Clustal Omega on the EBI server (3). Amino acid sequences of TEN used in the alignment were retrieved from the UniProtKB database (4) using the following IDs: R4IT35 *Ogataea polymorpha*, Q06163 *Saccharomyces cerevisiae* (strain ATCC 204508 / S288c), O13339 *Schizosaccharomyces pombe* (strain 972 / ATCC 24843), Q6BUF6 *Debaryomyces hansenii* (strain ATCC 36239 / CBS 767 / JCM 1990 / NBRC 0083 / IGC 2968), Q9P8T3 *Candida albicans,* B8YR05 *Strongylocentrotus purpuratus*, E9GVZ2 *Daphnia pulex*, J7SF03 *Helobdella robusta*, T2MJ53 *Hydra vulgaris* (Hydra), Q9DE32 *Xenopus laevis* (African clawed frog), K7G1G5 *Pelodiscus sinensis* (Chinese softshell turtle), Q4KTA7 *Takifugu rubripes* (Fugu fish), Q1PS67 *Oryzias latipes* (Japanese Killifish), Q537V4 *Gallus gallus* (Chicken), U3JHI5 *Ficedula albicollis* (Collared flycatcher), O14746 *Homo sapiens* (Human), Q673L6 *Rattus norvegicus* (Rat), H0VTM5 *Cavia porcellus* (Guinea pig), B5TFN0 *Ostreococcus tauri* (Green alga), D7G237 *Ectocarpus siliculosus* (Brown alga), Q9SPU7 *Arabidopsis thaliana*, Q1AN55 *Iris tectorum* (Iris), Q1EG34 *Zea mays* (Maize), Q8LKW0 *Oryza sativa* subsp. *Japonica* (Rice), B5B378 *Carica papaya* (Papaya), Q962F9 *Cryptosporidium parvum*, Q22ZB5 *Tetrahymena thermophile*, Q9GRC5 *Paramecium caudatum*, Q8MUQ8 *Paramecium tetraurelia*, O00939 *Euplotes aediculatus*, O76332 *Oxytricha trifallax*, A0A078A025 *Stylonychia lemnae*.

Microscale Thermophoresis

The binding affinity of the oligonucleotides to the protein was studied with the Microscale Thermophoresis method using a Monolith NT.115 (blue/green, NanoTemper Technologies) instrument with detection via the green channel. FAM label was inserted into the 5'-end of DNA oligonucleotides corresponding to the DNA strands of ligands E4 and E8 (Table 4). Prior the measurements they were dissolved in H_2O. The pH of the solutions was adjusted to 7.0. All experiments were conducted in the binding buffer (20 mM Na-phosphate buffer, pH 7.0, 50 mM NaCl) using a constant concentration of the FAM-labeled oligonucleotide ligands (50 nM) and 1:1 serial dilutions of each protein in the range of 18 nM to 0.6 mM. Oligonucleotide-protein mixtures were incubated for 20 min before loading into capillaries and introduction

into the MST instrument. Measurements were performed in standard treated capillaries (NanoTemper Technologies #MO-K002) at 25ºC using 100% infrared laser power and 40% LED power. Fitting of a sigmoidal curve into the experimental data and the determination of the dissociation constant (K_d) from the law of mass action was carried out using the NTAnalysis software (NanoTemper Technologies).

Labeled hpTEN binding to non-labeled E8 oligonucleotide was studied using the same parameters, but the protein was labeled with the GREEN-NHS (Amine Reactive) Labeling Kit (NanoTemper Technologies # MO-L002) following the manufacturer's instructions.

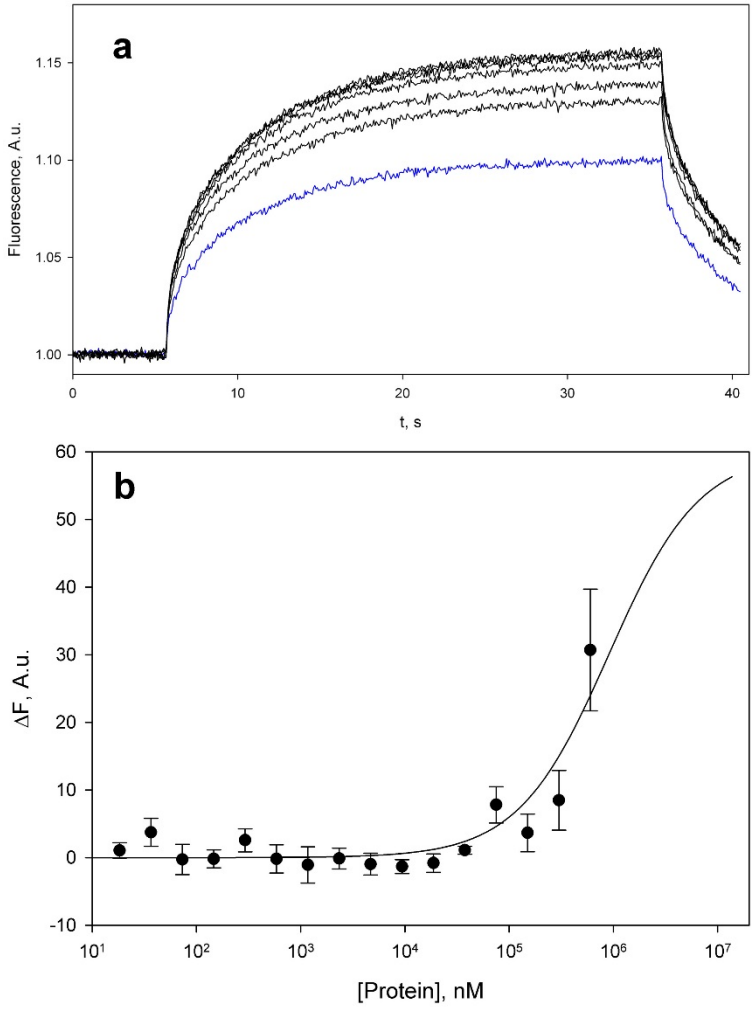

Figure S1. Example of titration curves obtained in the Microscale Thermophoresis experiments. (a) Time traces obtained for the titration of FAM-labeled fork E8 with the wild-type hpTEN. (b) Thermophoresis titration of FAM-labeled ssDNA with the wild-type hpTEN. The drawn curve corresponds to the following parameters: K_d,= 0.9 mM, Δ F_{max}=60 A.u.

Molecular modeling

The three dimensional structures of hpTERT fragment 209-783 (hpTERT-ring) and hTEN were modeled using the I-Tasser online server (5). The generated models were ranked according to their C-score (quantitative measure of the confidence), TM score (quantitative assessment of protein structural similarity) and RMSD. For the TERT ring all ten threading templates found by I-Tasser were crystal structures of TERT from *Tribolium castaneum* (tcTERT, PDB ID codes: 3DU5, 3DU6 (6), 3KYL (7) and 5CQG (8)). Despite the low sequence identity of the two proteins (22%), the normalized Z-score for the

best threading template was 5.8. The best scoring model had a C-score of -0.31 signifying a good confidence of the prediction. The PDB structure 3DU6 was identified by I-Tasser as the closest structural homolog to the obtained model with a TM-score of 0.833 and the RMSD of the backbone atoms of 1.10 Å (the percent of structurally aligned residues was 0.846). The positions of side-chains of aspartate residues 472, 616 and 617 in the hpTERT ring match those of the catalytic aspartate residues 251, 343, and 344 in tcTERT with all-atoms RMSD of 0.57 Å. The best scoring model of hpTERT-ring was used for further modeling. For the structure prediction of hTEN the NMR structure of hpTEN (a representative conformation) was provided to I-Tasser as a template. The best scoring model of hTEN (with a C-score of -0.60 signifying a good confidence of the prediction) had an RMSD with the template structure of 1.36 Å (at the percent of structurally aligned residues of 0.861). This model was used for the structure-based sequence alignment. The structure of ttTEN (PDB ID code 2B2A) (9) was identified by I-Tasser as the closest topological homolog with a TM score of 0.548. There was no significant structural homology found between this model of hTEN and ttTEN. The RMSD was higher than 3Å (calculated for the percent of structurally aligned residues of 0.698). For comparison, structure prediction of hTEN using hpTEN structure as a template (presented in this study, PDB ID code 5LGF) resulted in a best scoring model with C-score of -0.86. In this case, the TM-score between the template and the model was 0.760 with the RMSD of 1.78 Å (at the percent of structurally aligned residues of 0.831).

The three dimensional coordinates of a heteroduplex DNA product – RNA template were generated using the UCSF Chimera package v. 1.10.2 (build 40686)(10) with the sequence corresponding to the telomeric repeat and the template region of telomerase RNA from *H. polymorpha*. 3D structures of other fragments of telomerase RNA were obtained using the RNAComposer server (11) and then combined in Chimera with the heteroduplex part to generate a number of possible conformations of the fork. To model the position of the fork in the central pore of TERT ring the structure 3KYL of tcTERT complexed with an RNA/DNA hairpin (7) was used. First the hpTERT-ring was superimposed to the protein part of tcTERT complex. The heteroduplex part of the fork was then superimposed to the heteroduplex part of a hairpin bound in tcTERT. All-atom least-squares superposition was carried out using Coot (12). A number of superposed variants were generated where the first nucleotide of a fork (3'-end of a DNA strand) corresponded to different nucleotides of a hairpin. The variant where the 3'-terminal nucleotide of DNA dT18 of a fork corresponded to a nucleotide dG24 of a hairpin had the lowest RMSD (0.46 Å) and the closest distance (2.93 Å) between the OD2 atom of Asp616 and the OP1 atom of dG1 phosphate. This model was inspected using Chimera and minor clashes with the residues of the central pore were eliminated. Conformations of single-stranded parts of the fork were adjusted to avoid clashes with the TERT ring and subsequently regularized using Coot. The position of hpTEN with respect to hpTERT ring and the fork was modeled in Chimera using the experimental data on NMR titration as structural restraints. Geometry of the final model was optimized in Coot and the overall quality was validated using Procheck (13) and the WhatCheck module of the WhatIf software suite (14). The images used in this work were generated using PyMOL and UCSF Chimera.

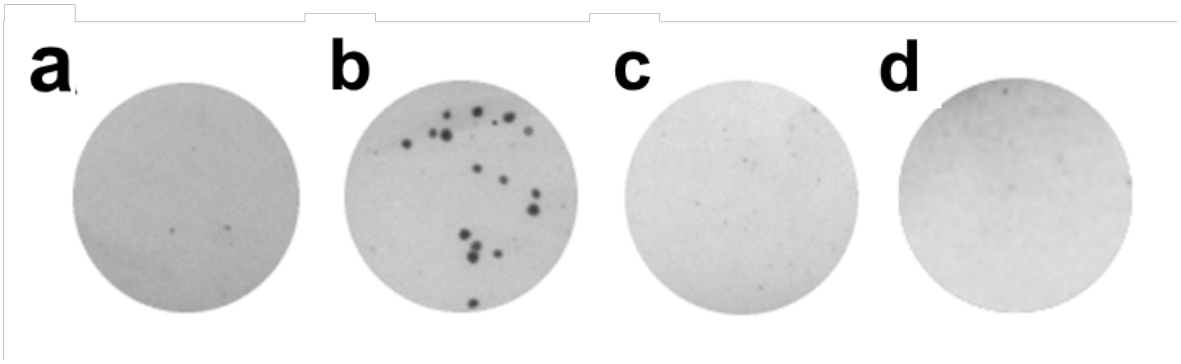

Figure S2. Plate images after transformation of the ΔhpTERT strain with shuttle vector carrying the gene of interest: (**a**) Empty vector. (**b**) The vector with wt hpTERT gene under control of the native promoter. (**c**) The vector with the TEN-deleted hpTERT gene (179-783 fragment of hpTERT) under control of the hpTERT promoter. (**d**) The vector with the TEN-deleted hpTERT gene (coding for 179-782 fragment of hpTERT) and TEN domain (1-153), each under control of the hpTERT promoter.

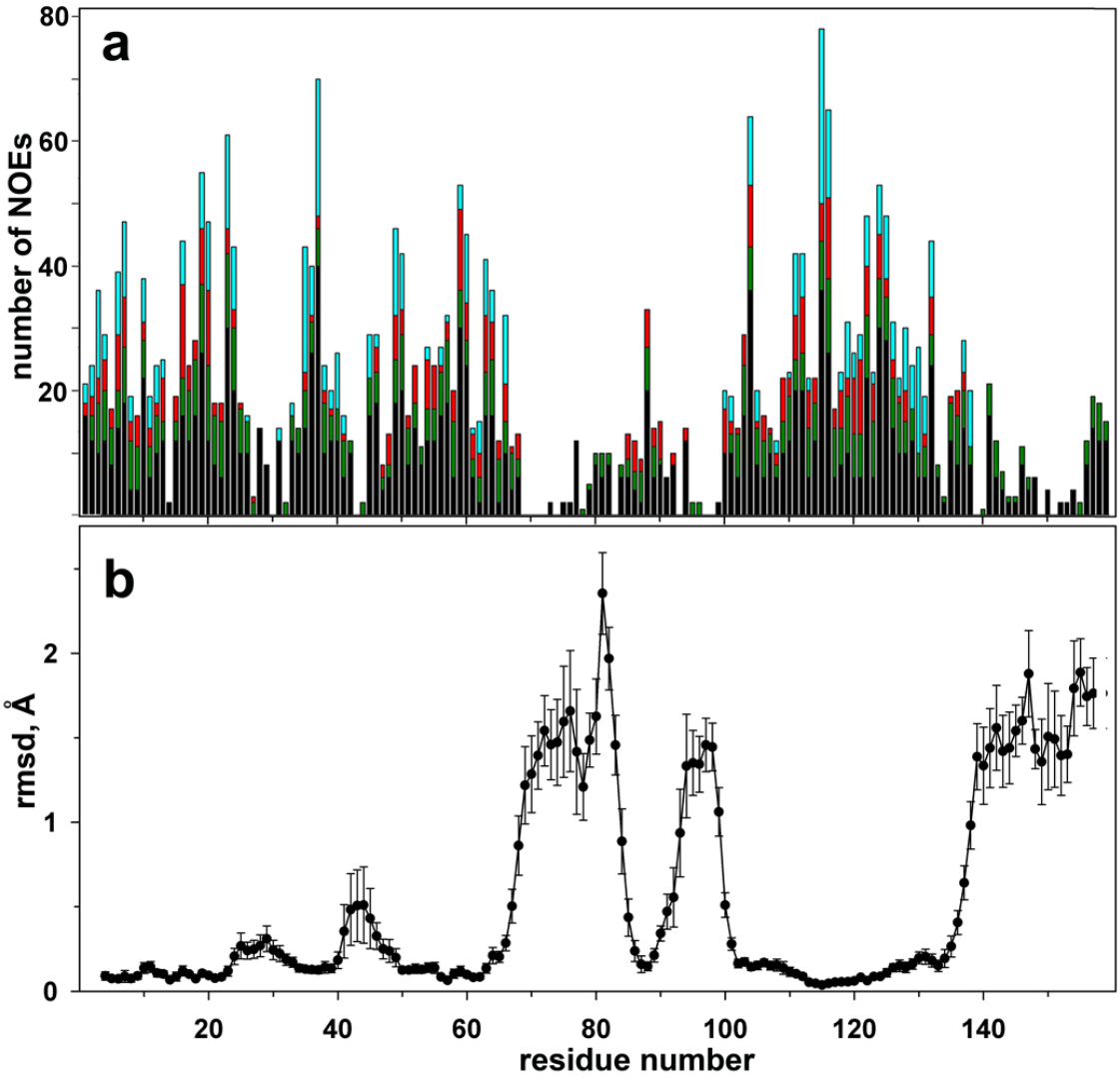

Figure S3. (**a**) NOE histogram giving the number of long-range (cyan), medium-range (red), sequential (green) and intra-residue (black) NOEs for each protein residue in the hpTEN. (**b**) RMSD values for the non-hydrogen atoms of each residue *i* after the pairwise superposition of the family of 20 NMR structures of hpTEN using the set of backbone atoms of four adjacent residues (*i*-2, *i*-1, *i*+1, and *i*+2).

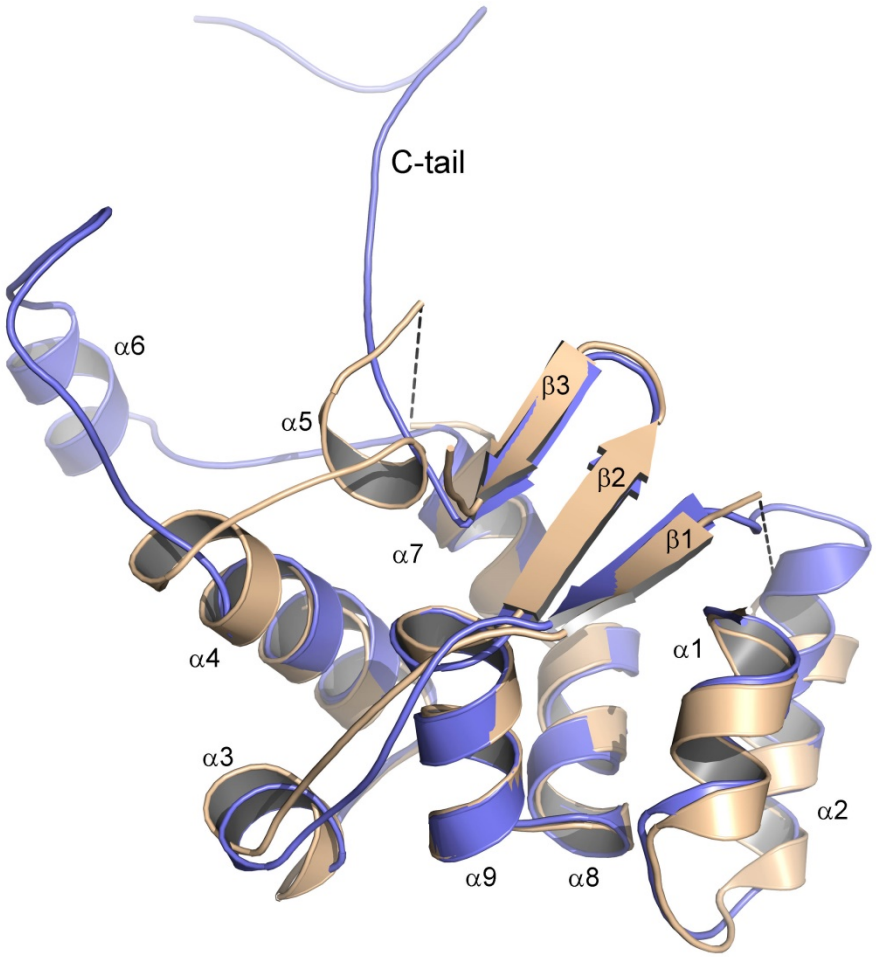

Figure S4. Superposition of solution (representative model in blue) and crystal (gold) structures of hpTEN.

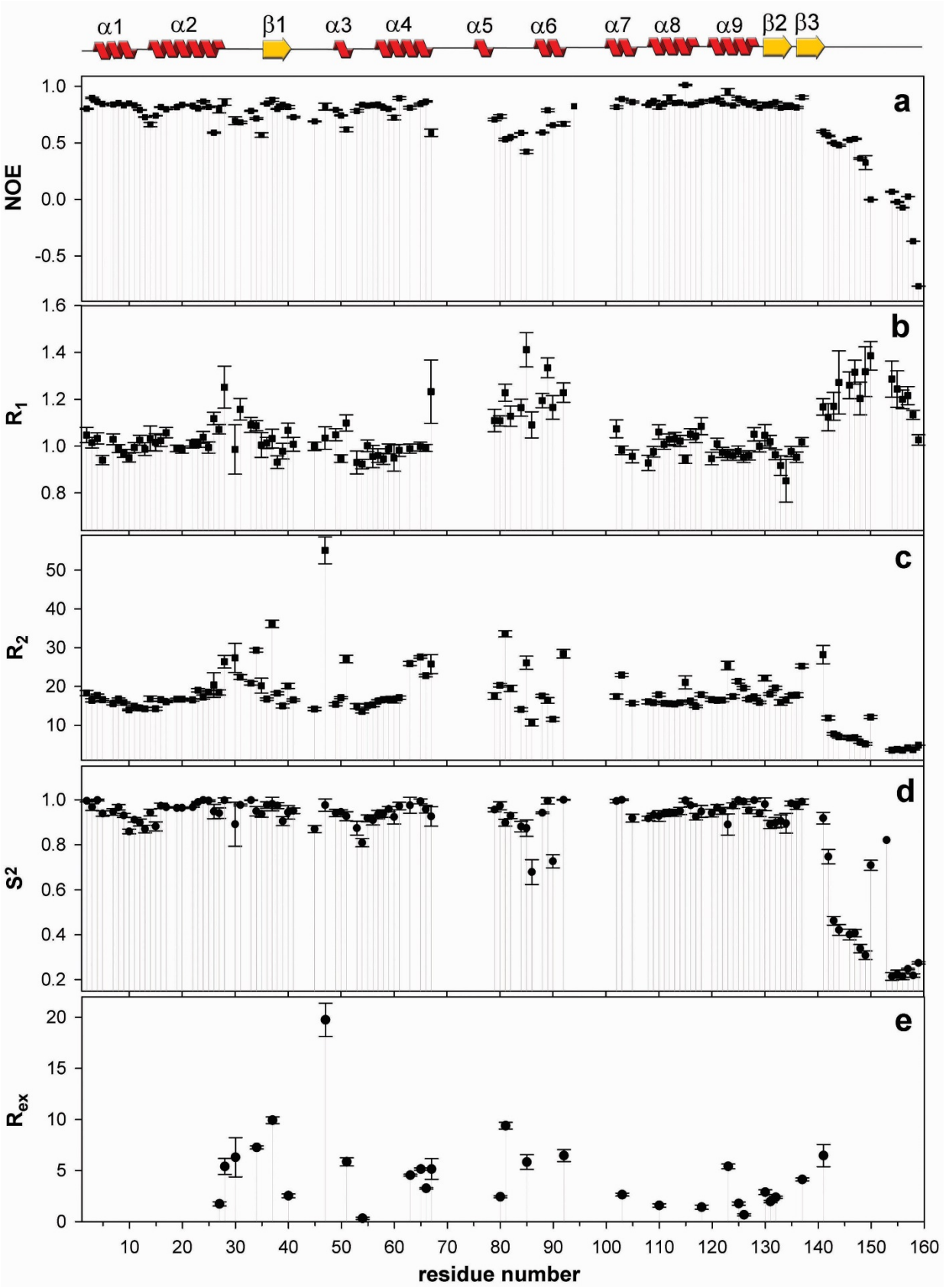

Figure S5. The relaxation parameters of the amide ^{15}N nuclei in hpTEN measured at 16.3 T and 298 K. Values of the heteronuclear ^{15}N,^{1}H-steady-state NOE are shown (**a**), longitudinal relaxation rate constant, R_1, (s^{-1}, **b**), transverse relaxation rate constant, R_2 (s^{-1}, **c**), the order parameter S^2 determined by model-free analysis (**d**) and chemical exchange R_{ex} contributions to the transverse relaxation rate constants (s^{-1}, **e**).

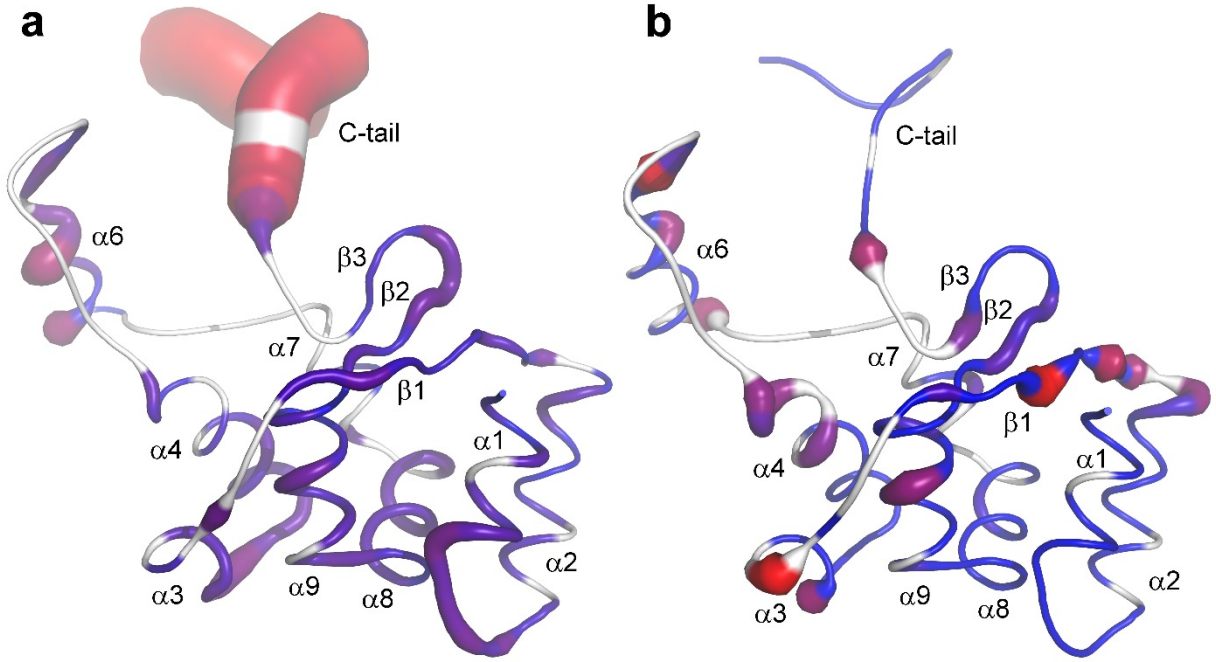

Figure S6. Dynamic and conformational behavior of the hpTEN. (**a**). A representative NMR model of hpTEN shown according to protein mobility on the ps-ns time scale. The color scheme represents the order parameters S^2 (blue for 1 and red for ~0.2). Residues with undetermined S^2 are colored in white. The thickness of the chain is proportional to the value (1- S^2) (the extent of the local amplitude of protein backbone motion) (**b**). A representative NMR structure of hpTEN shown according to protein mobility on the ms time scale. Colors represent the values of the chemical exchange (R_{ex}) contribution to the transverse relaxation rate constant (blue for 0 and red for values higher than 10). The thickness of the chain is proportional to the value of R_{ex}.

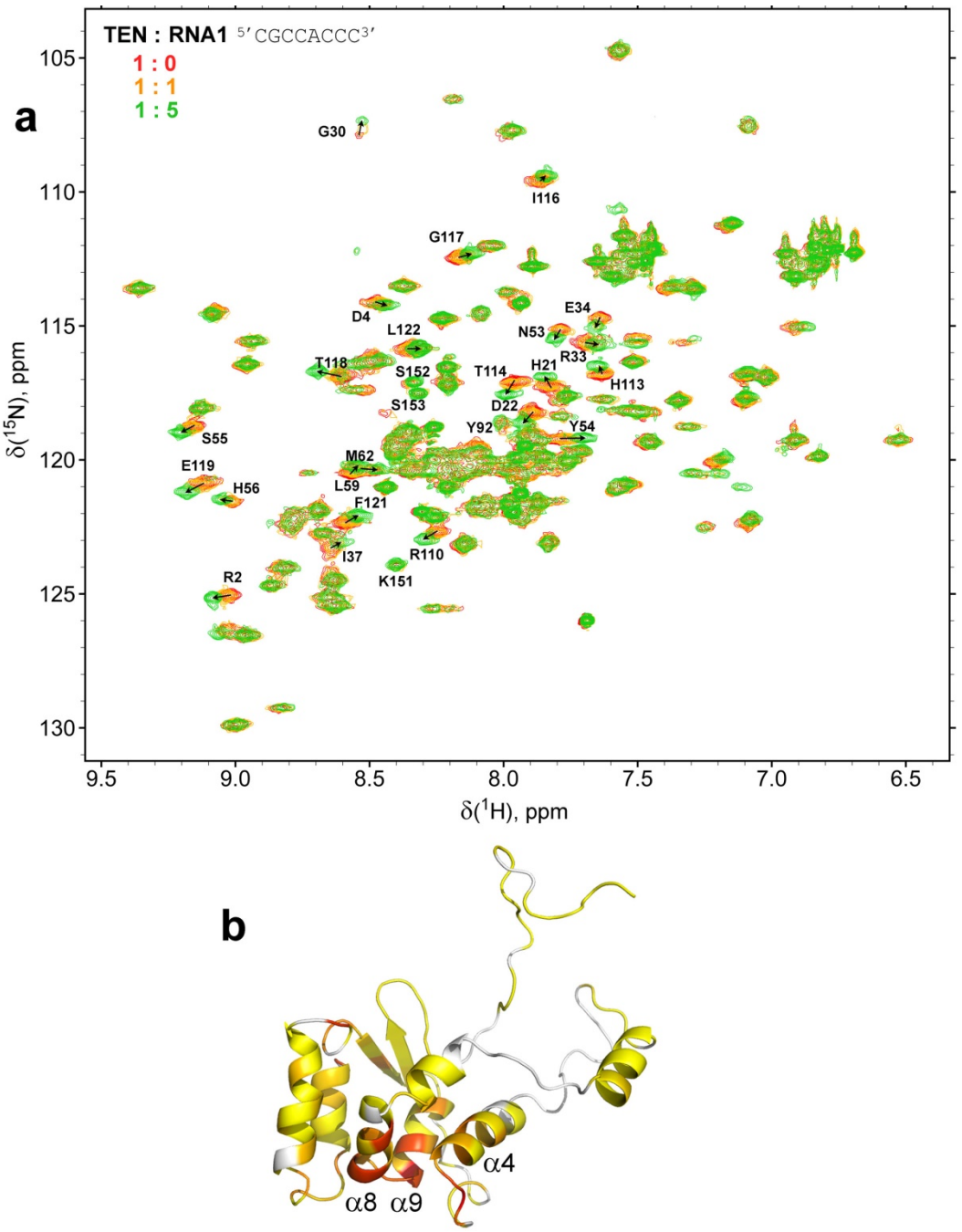

Figure S7. NMR studies of hpTEN titration with ssRNA fragment **E1** (represents single telomeric template, Table 4): (**a**) overlay of ^{1}H-^{15}N HSQC spectra of hpTEN (0.2 mM) with different amounts of **E1**. The spectrum for free hpTEN is in red, for hpTEN in the presence of 1 eq **E1** in orange, and for hpTEN in the presence of 5 eq **E1** in green. The peaks shifted significantly are labeled and shown by arrows; (**b**) mapping of the hpTEN residues affected by the binding of **E1**. Ribbon diagram is colored according to the RMSD values of ^{1}H and ^{15}N chemical shifts of amide groups in the protein backbone between free hpTEN and hpTEN in the presence of 5 eq **E1**. Yellow color is used for the regions that do not respond to **E1** binding, while red color indicates regions with maximum changes of the RMSD values upon **E1** binding. Residues that are not observed in ^{1}H-^{15}N HSQC spectrum are colored in white.

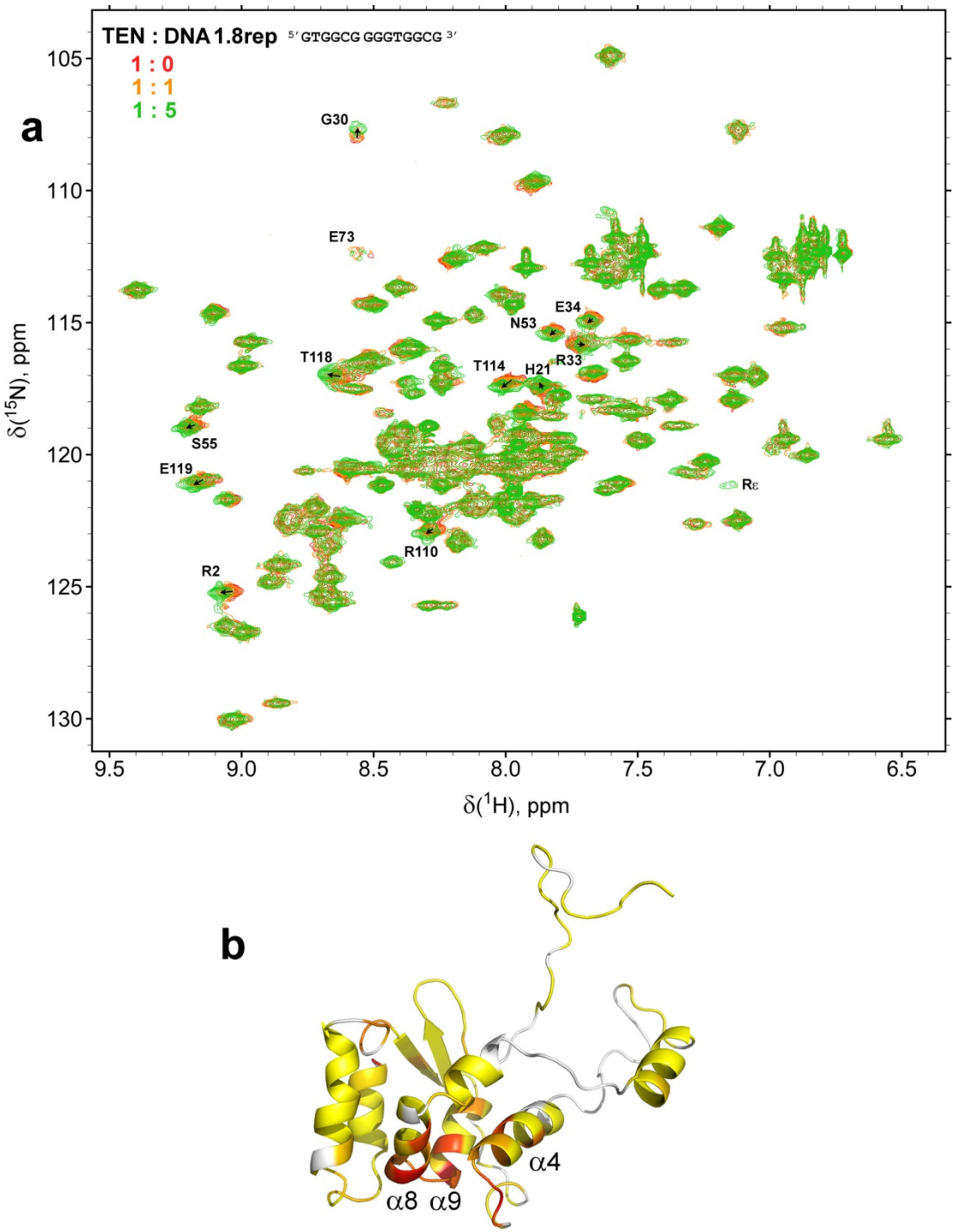

Figure S8. NMR studies of hpTEN titration with ssDNA fragment **E2** (represents ~1.8 telomeric repeats, Table 4): (**a**) overlay of ^{1}H-^{15}N HSQC spectra of hpTEN (0.2 mM) with variable amount of **E2**. The spectrum for free hpTEN is in red, for hpTEN in the presence of 1 eq **E2** in orange, and for hpTEN in the presence of 5 eq **E2** in green. The peaks shifted significantly are labeled and shown by arrows; (**b**) mapping of the hpTEN residues affected by the binding of **E2**. Ribbon diagram is colored according to the RMSD values of ^{1}H and ^{15}N chemical shifts of amide groups in the protein backbone between free hpTEN and hpTEN in the presence of 5 eq **E2**. Yellow color is used for the regions that do not respond to **E2** binding, while red color indicates regions with maximum changes of the RMSD values upon **E2** binding. Residues that are not observed in ^{1}H-^{15}N HSQC spectrum are colored in white.

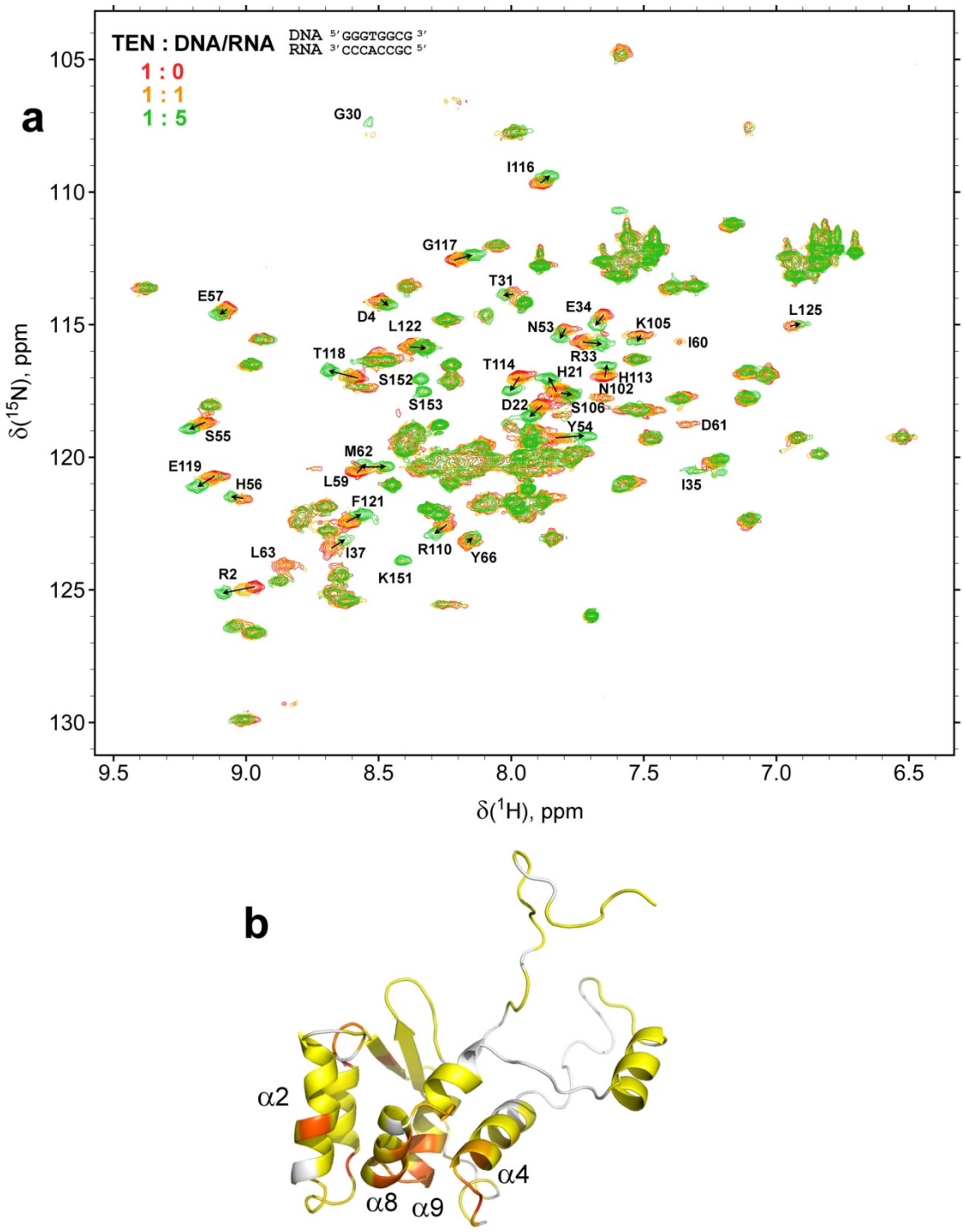

Figure S9. NMR studies of hpTEN titration with RNA-DNA heteroduplex **E3** (represents single telomeric repeat, Table 4): (**a**) overlay of ^{1}H-^{15}N HSQC spectra of hpTEN (0.2 mM) with variable amount of **E3**. The spectrum for free hpTEN is in red, for hpTEN in the presence of 1 eq **E3** in orange, and for hpTEN in the presence of 5 eq **E3** in green. The peaks shifted significantly are labeled and shown by arrows; (**b**) mapping of the hpTEN residues affected by the binding of **E3**. Ribbon diagram is colored according to the RMSD values of ^{1}H and ^{15}N chemical shifts of amide groups in the protein backbone between free hpTEN and hpTEN in the presence of 5 eq **E3**. Yellow color is used for the regions that do not respond to **E3** binding, while red color indicates regions with maximum changes of the RMSD values upon **E3** binding. Residues that are not observed in ^{1}H-^{15}N HSQC spectrum are colored in white.

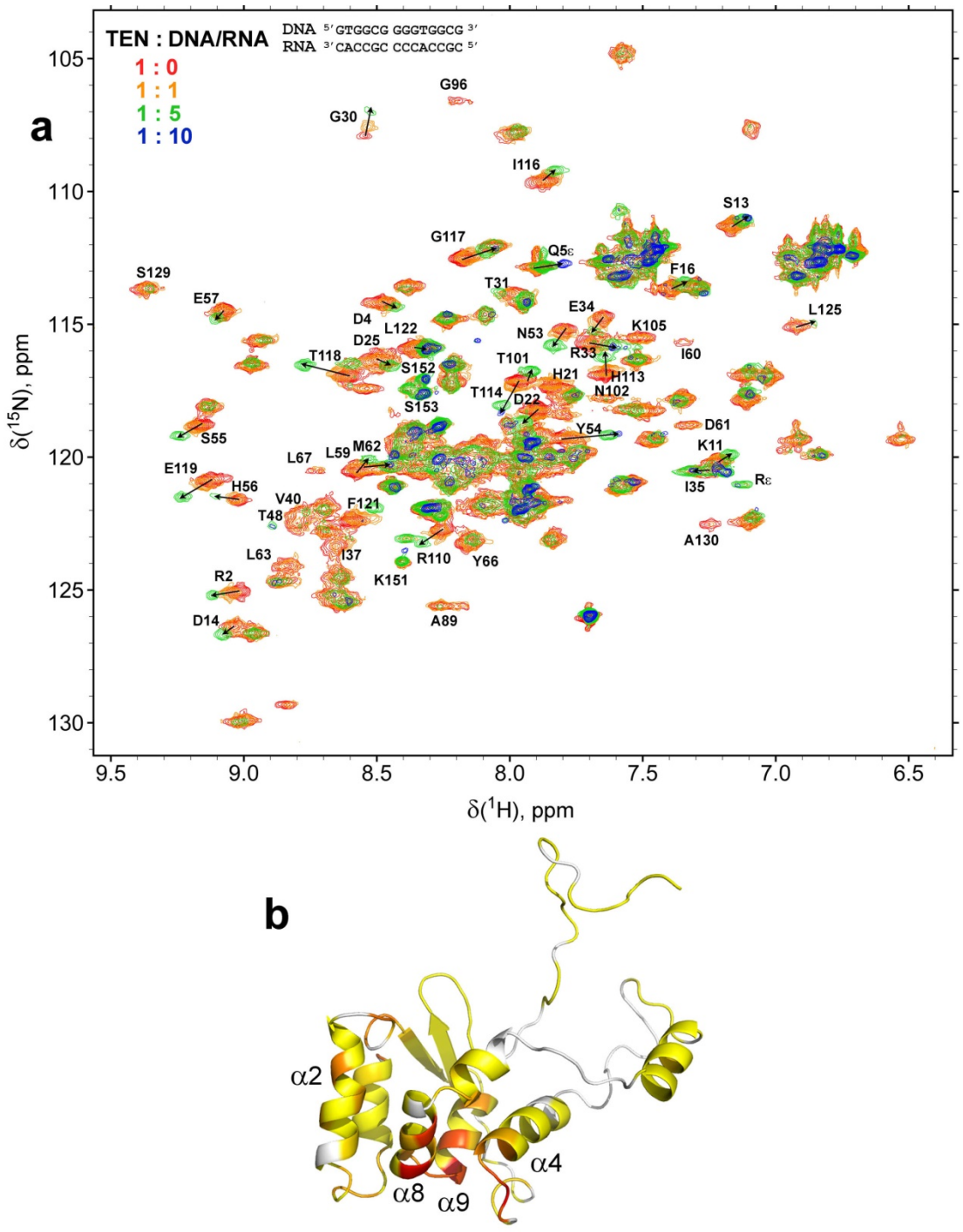

Figure S10. NMR studies of hpTEN titration with RNA-DNA heteroduplex **E4** (represents ~1.8 telomeric repeats, Table 4): (**a**) overlay of ^{1}H-^{15}N HSQC spectra of hpTEN (0.2 mM) with variable amount of **E4**. The spectrum for free hpTEN is in red, for hpTEN in the presence of 1 eq **E4** in orange, in the presence of 5 eq **E4** in green and in the presence of 10 eq **E4** in blue. The peaks shifted significantly are labeled and shown by arrows; (**b**) mapping of the hpTEN residues affected by the binding of **E4**. Ribbon diagram is colored according to the RMSD values of ^{1}H and ^{15}N chemical shifts of amide groups in the protein backbone between free hpTEN and hpTEN in the presence of 5 eq **E4**. Yellow color is used for the regions that do not respond to **E4** binding, while red color indicates regions with maximum changes of the RMSD values upon **E4** binding. Residues that are not observed in ^{1}H-^{15}N HSQC spectrum are colored in white.

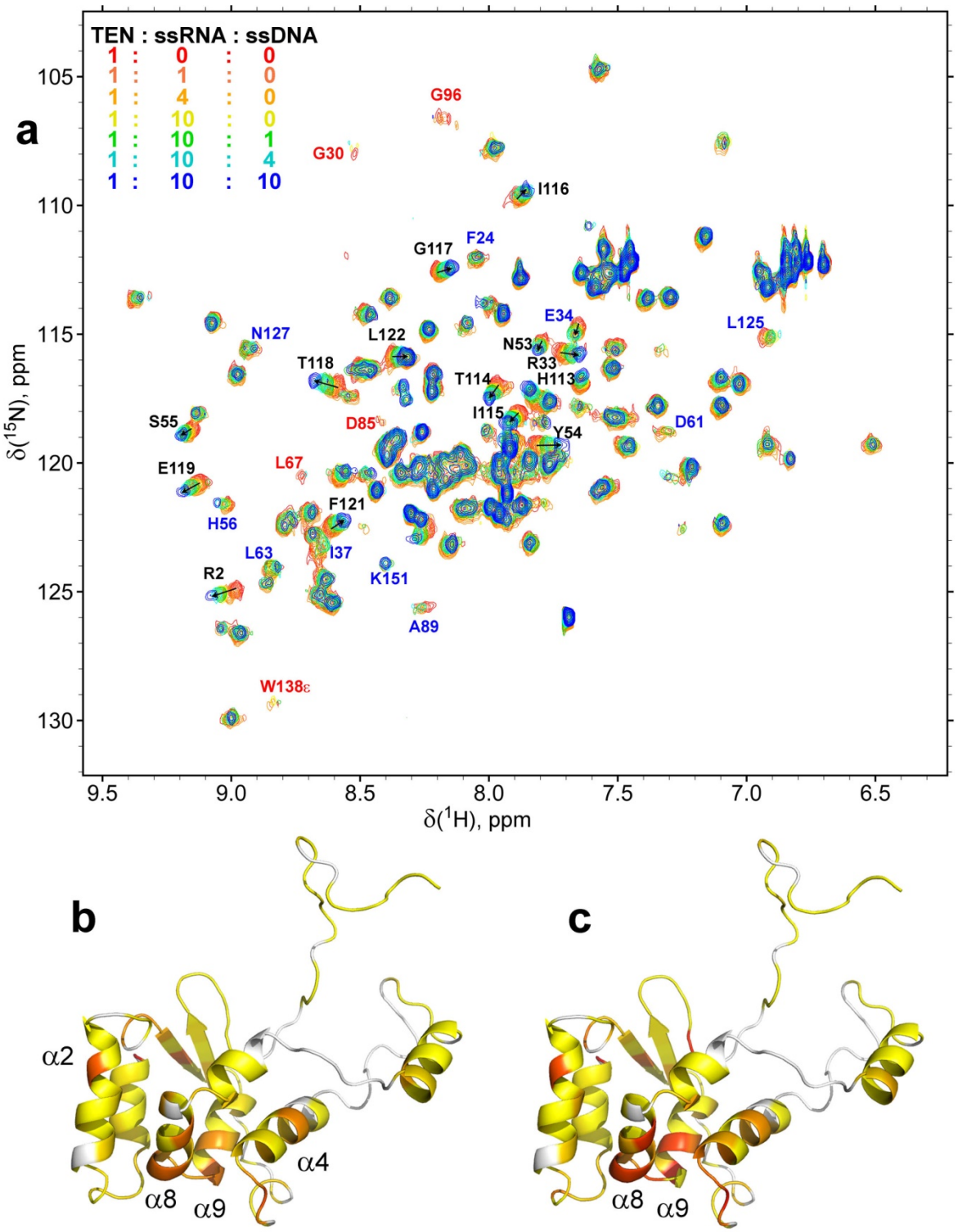

Figure S11. NMR studies of hpTEN titration with ssRNA **E5** followed by ssDNA **E6** (Table 4): (**a**) overlay of ^{1}H-^{15}N HSQC spectra of hpTEN (0.2 mM) with variable amounts of **E5** and **E6**. The spectrum for free hpTEN is in red, for hpTEN in the presence of 1 eq **E5** in dark orange, in the presence of 4 eq **E5** in orange, in the presence of 10 eq **E5** in yellow, in the presence of 10 eq **E5** and 1 eq **E6** in green, in the presence of 10 eq **E5** and 4 eq **E6** in cyan, and for hpTEN in the presence of 10 eq **E5** and 10 eq **E6** in blue. The peaks shifted gradually upon addition of **E5** and **E6** are labeled in black. The peaks shifted mainly upon the addition of **E6** are labeled red; (**b**) mapping of the hpTEN residues affected by the binding of **E5**. Ribbon diagram is colored according to the RMSD values of ^{1}H and ^{15}N chemical shifts of amide groups in the protein backbone between free hpTEN and hpTEN in the presence of 5 eq **E5**; (**c**) mapping of the hpTEN residues in a complex with **E5** affected by the subsequent binding of **E6**. Ribbon diagram is colored according to the RMSD values of ^{1}H and ^{15}N chemical shifts of amide groups in the

protein backbone between hpTEN in the presence of 10 eq **E5** and hpTEN in the presence of 10 eq **E5** and 4 eq **E6**. Yellow color in (**b**) and (**c**) indicates the regions that do not respond to **E5** (or **E6**) binding, red color shows regions with the maximum changes of the RMSD values after **E5** (or **E6**) binding. Residues that are not observed in ^{1}H-^{15}N HSQC spectrum are colored in white.

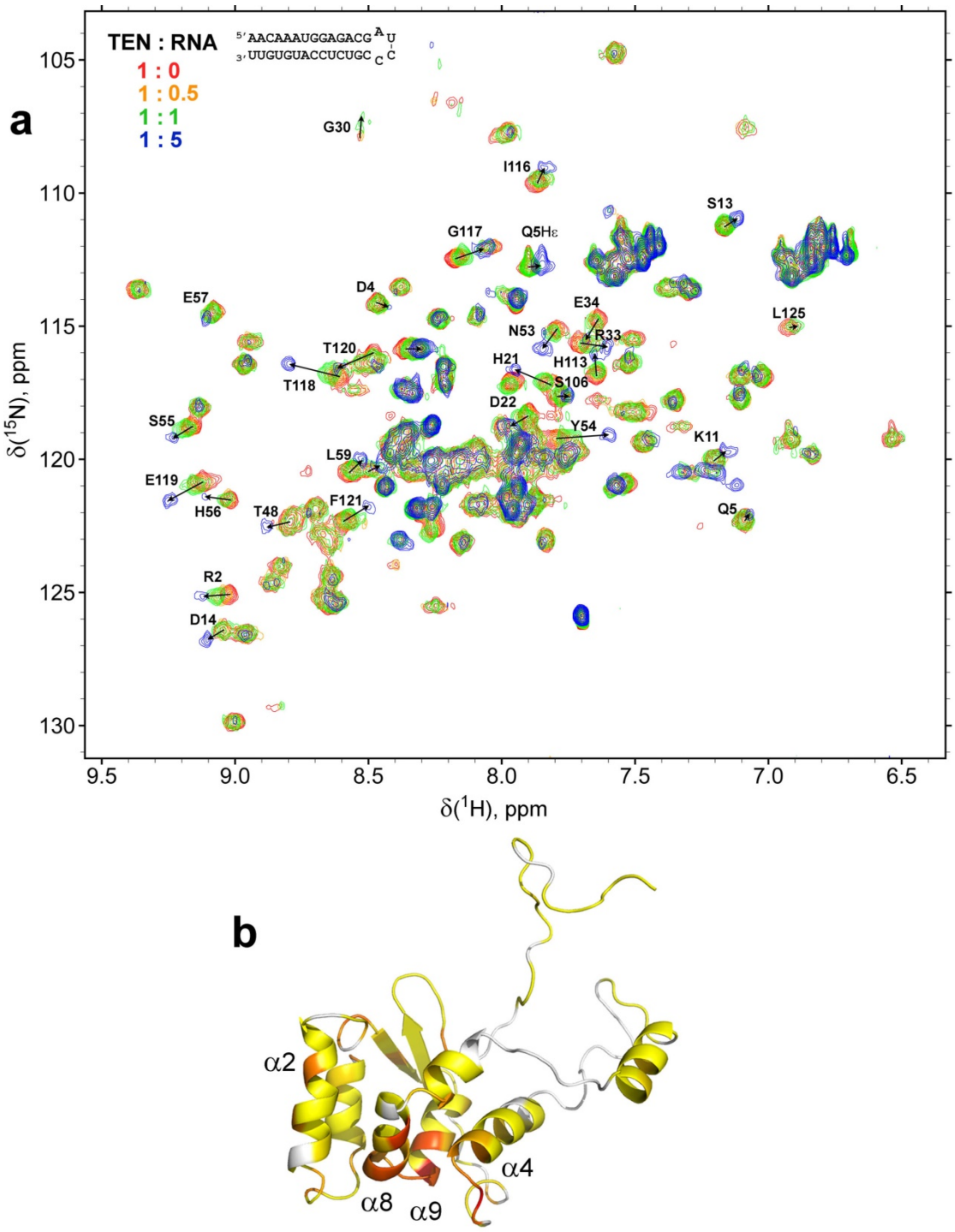

Figure S12. NMR studies of hpTEN titration with RNA hairpin **E11** (Table 4): (**a**) overlay of ^{1}H-^{15}N HSQC spectra of hpTEN (0.2 mM) with variable amount of **E11**. The spectrum for free hpTEN is in red, in the presence of 0.5 eq **E11** in orange, in the presence of 1 eq **E11** in green and in the presence of 5 eq **E11** in blue. The peaks shifted significantly labeled and shown by arrows; (**b**) mapping of the hpTEN residues affected by the binding of **E11**. Ribbon diagram is colored according to the RMSD values of ^{1}H and ^{15}N chemical shifts of amide groups in the protein backbone between free hpTEN and hpTEN in the presence of 5 eq **E11**. Yellow color indicates the regions that do not respond to **E11** binding, red color shows regions with the maximum changes of the RMSD values after **E11** binding. Residues that are not observed in ^{1}H-^{15}N HSQC spectrum are colored in white.

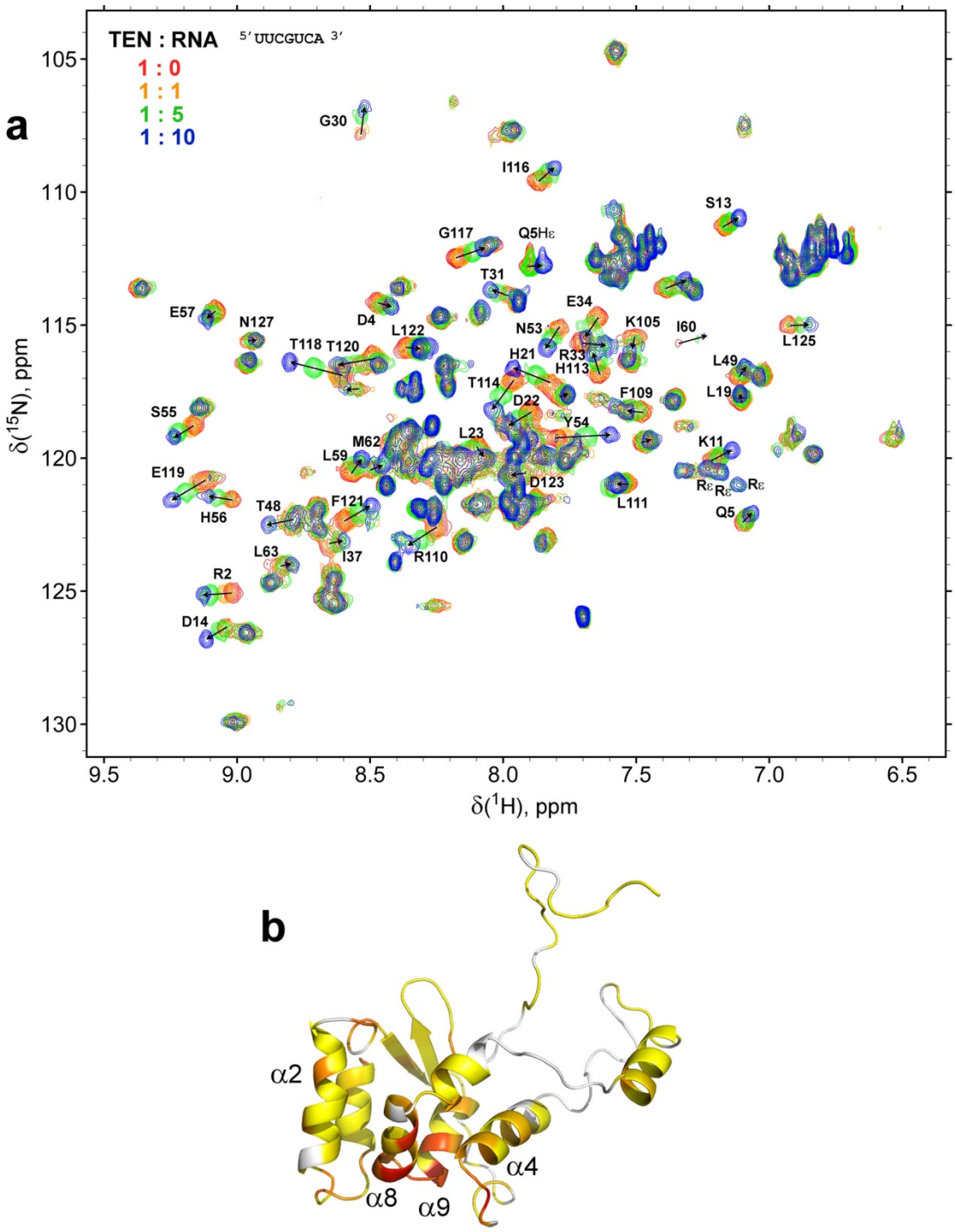

Figure S13. NMR studies of hpTEN titration with the RNA upstream fragment **E10** (Table 4): (**a**) overlay of ^{1}H-^{15}N HSQC spectra of hpTEN (0.2 mM) with variable amounts of **E10**. The spectrum for free hpTEN is in red, in the presence of 0.5 eq **E10** in orange, in the presence of 5 eq **E10** and in green and in the presence of 10 eq **E10** in blue. The peaks shifted significantly labeled and shown by arrows; (**b**) mapping of the hpTEN residues affected by the binding of **E10**. Ribbon diagram is colored according to the RMSD values of ^{1}H and ^{15}N chemical shifts of amide groups in the protein backbone between free hpTEN and hpTEN in the presence of 5 eq **E10**. Yellow color indicates the regions that do not respond to **E10** binding, red color shows regions with the maximum changes of the RMSD values after **E10** binding. Residues that are not observed in ^{1}H-^{15}N HSQC spectrum are colored in white.

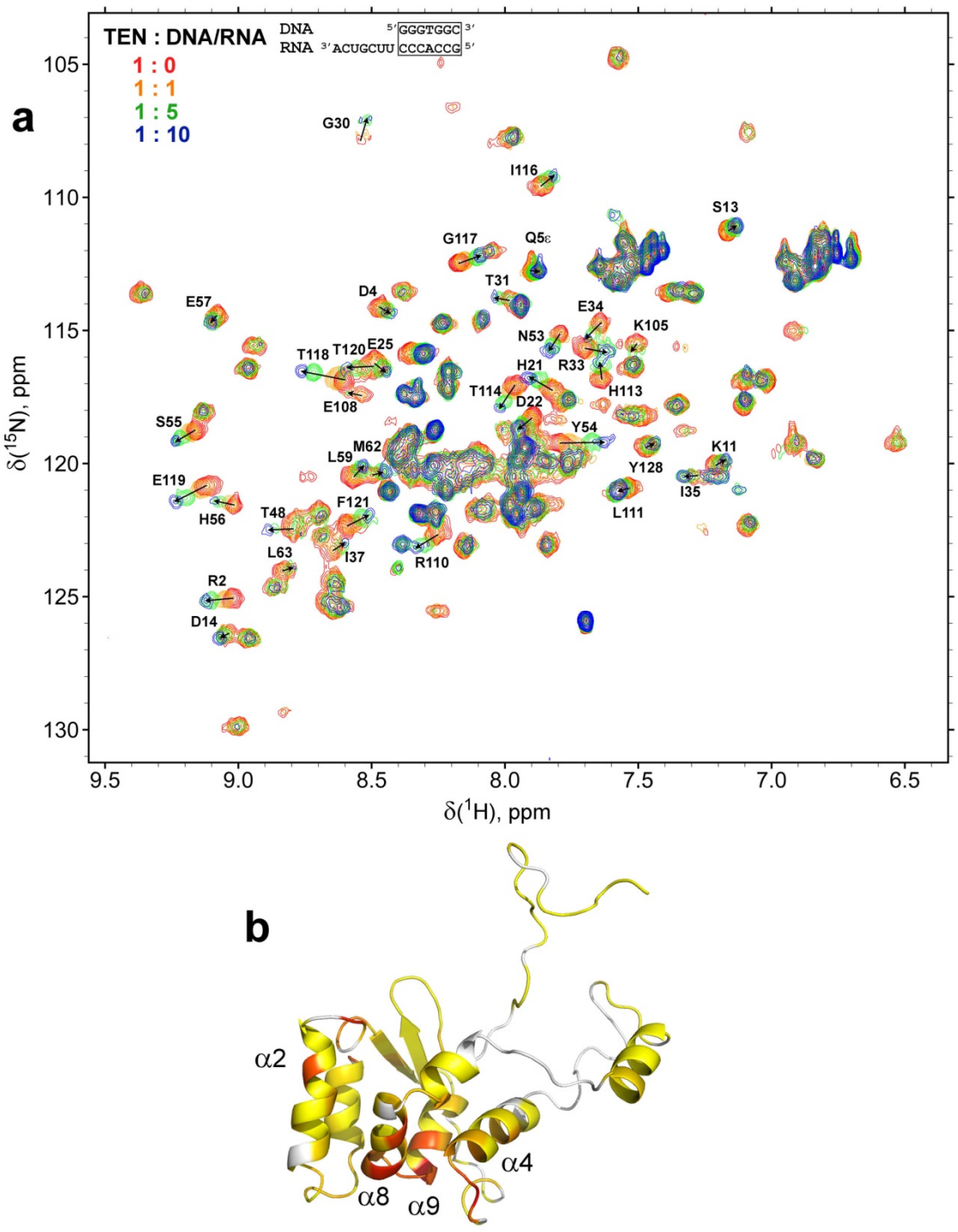

Figure S14. Results of NMR studies of hpTEN titration with the RNA-DNA half fork heteroduplex **E9** (Table 4): (**a**) overlay of ^{1}H-^{15}N HSQC spectra of hpTEN (0.2 mM) with variation of the **E9** amount. The spectrum for free hpTEN is in red, in the presence of 0.5 eq **E9** in orange, in the presence of 5 eq **E9** and in green and in the presence of 10 eq **E9** in blue. The peaks shifted significantly labeled and shown by arrows; (**b**) mapping of the hpTEN residues affected by the binding of **E9**. Ribbon diagram is colored according to the RMSD values of ^{1}H and ^{15}N chemical shifts of amide groups in the protein backbone between free hpTEN and hpTEN in the presence of 5 eq **E9**. Yellow color indicates the regions that do not respond to **E9** binding, red color shows regions with the maximum changes of the RMSD values after **E9** binding. Residues that are not observed in ^{1}H-^{15}N HSQC spectrum are colored in white.

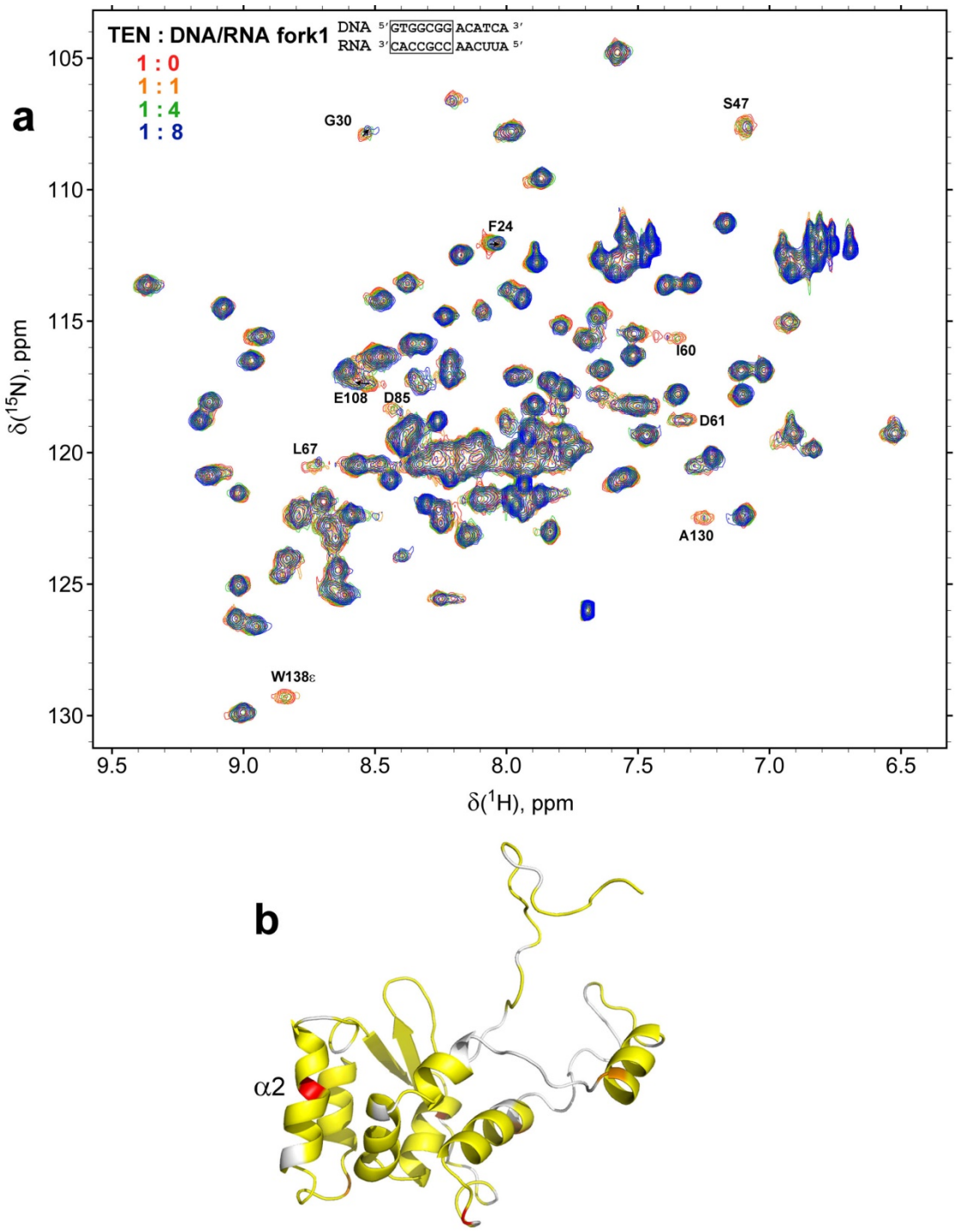

Figure S15. NMR studies of hpTEN titration with the RNA-DNA fork **E7** in a reversed orientation in comparison with the natural bifurcated duplex in telomerase (Table 4): (**a**) overlay of ^{1}H-^{15}N HSQC spectra of hpTEN (0.2 mM) with variable amount of **E7**. The spectrum for free hpTEN is in red, in the presence of 0.5 eq **E7** in orange, in the presence of 5 eq **E7** and in green and in the presence of 8 eq **E7** in blue. The peaks shifted significantly labeled and shown by arrows; (**b**) mapping of the hpTEN residues affected by the binding of **E7**. Ribbon diagram is colored according to the RMSD values of ^{1}H and ^{15}N chemical shifts of amide groups in the protein backbone between free hpTEN and hpTEN in the presence of 5 eq **E7**. Yellow color indicates the regions that do not respond to **E7** binding, red color shows regions with the maximum changes of the RMSD values after **E7** binding. Residues that are not observed in ^{1}H-^{15}N HSQC spectrum are colored in white.

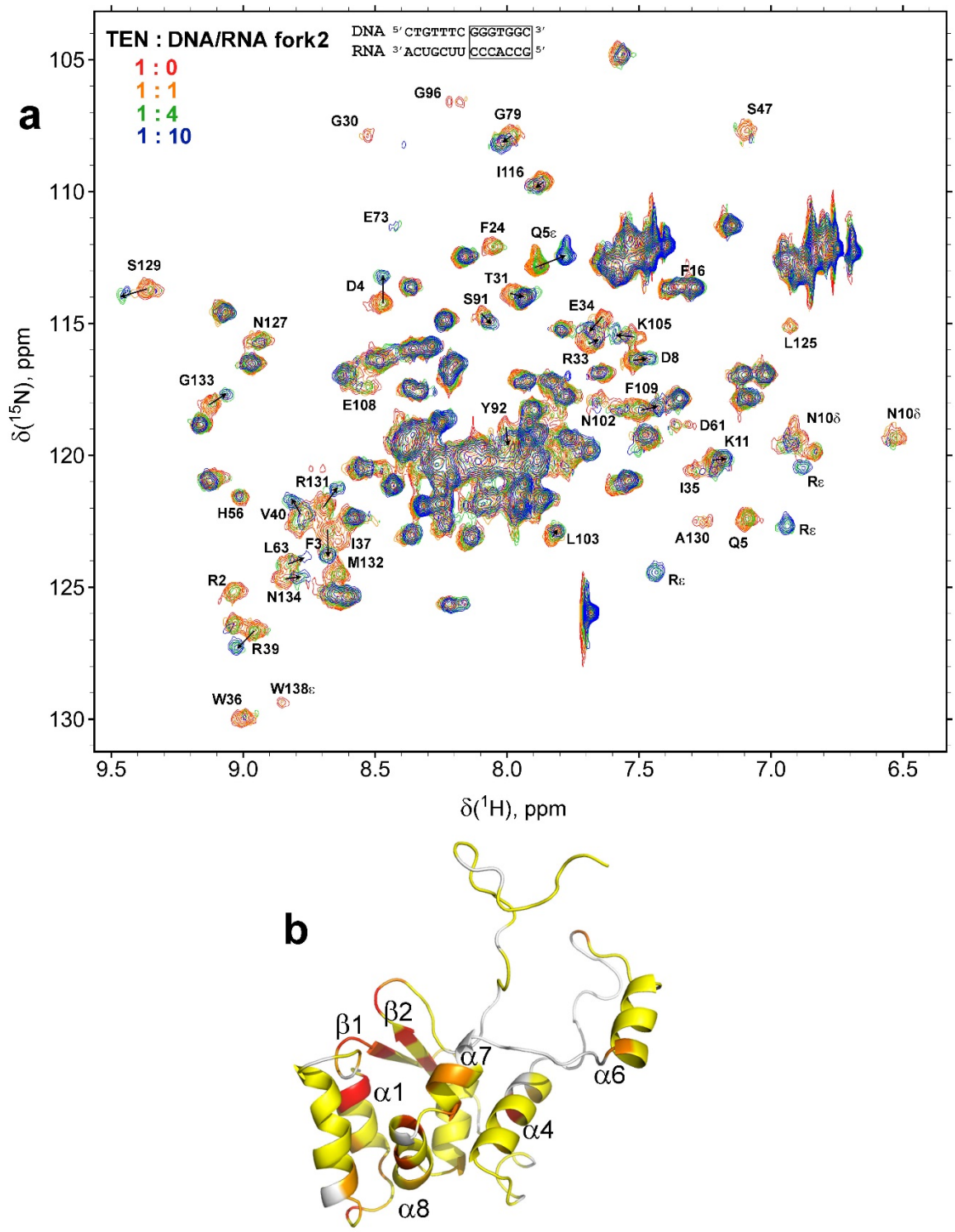

Figure S16. NMR studies of hpTEN titration with the RNA-DNA fork **E8** in a direct (native) orientation (Table 4): (**a**) overlay of ^{1}H-^{15}N HSQC spectra of hpTEN (0.2 mM) with variable amount of **E8**. The spectrum for free hpTEN is in red, in the presence of 1 eq **E8** in orange, in the presence of 4 eq **E8** in green and in the presence of 10 eq **E8** in blue. The peaks shifted significantly labeled and shown by arrows; (**b**) mapping of the hpTEN residues affected by the binding of **E8**. Ribbon diagram is colored according to the RMSD values of ^{1}H and ^{15}N chemical shifts of amide groups in the protein backbone between free hpTEN and hpTEN in the presence of 5 eq **E8**. Yellow color indicates the regions that do not respond to **E8** binding, red color shows regions with the maximum changes of the RMSD values after **E8** binding. Residues that are not observed in ^{1}H-^{15}N HSQC spectrum are colored in white.

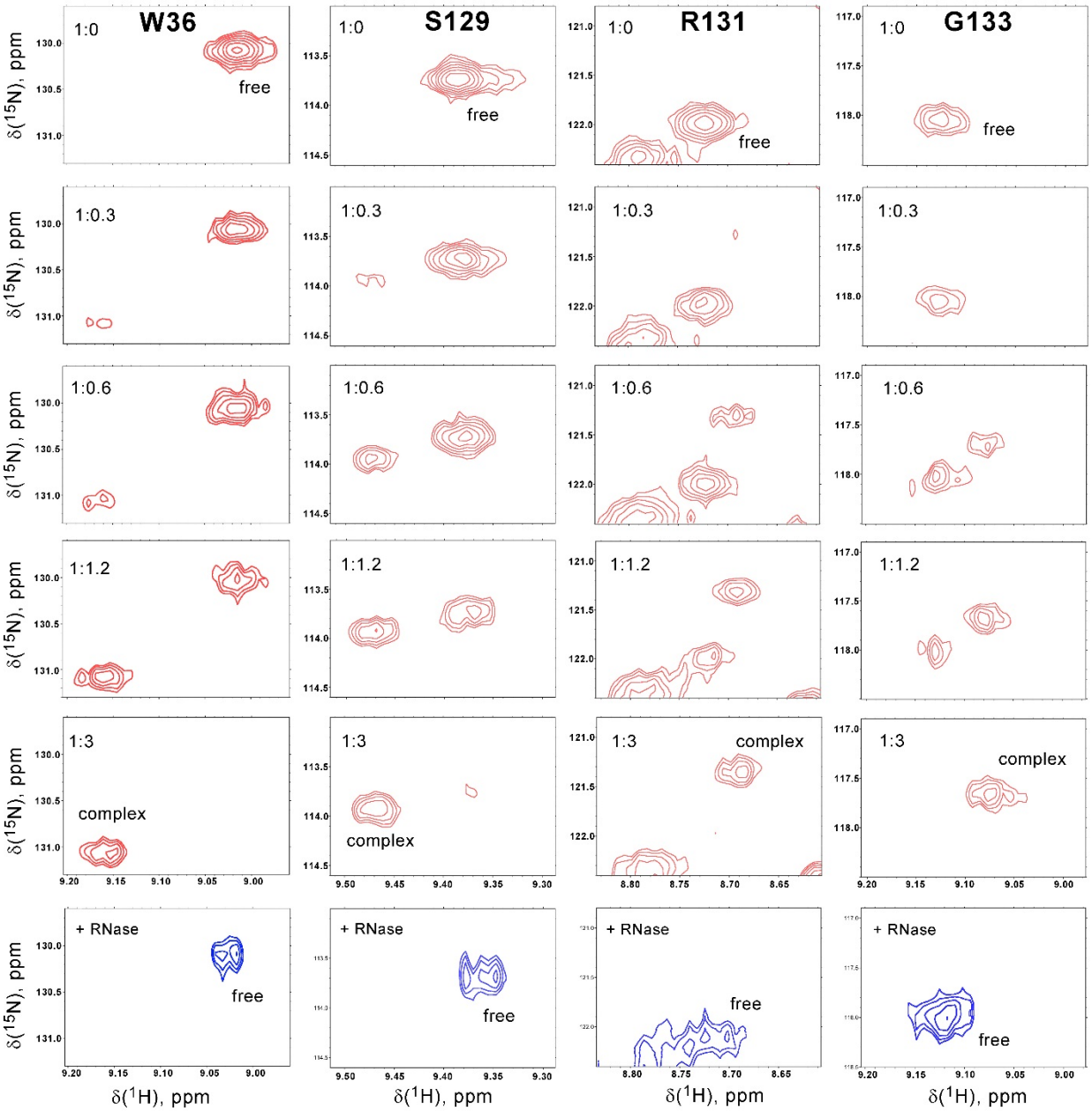

Figure S17. Representative fragments of ^{15}N-^{1}H HSQC spectra of hpTEN recorded during the protein titration by the RNA-DNA fork **E8** (Table 4). Shown are backbone amide residues W36, S129, R131 and G133. Appearance of the two separate sets of signals indicates a slow exchange rate between free protein and its complex with fork **E8** (shown by red). Addition of RNase returns resonances to the positions of free protein (blue).

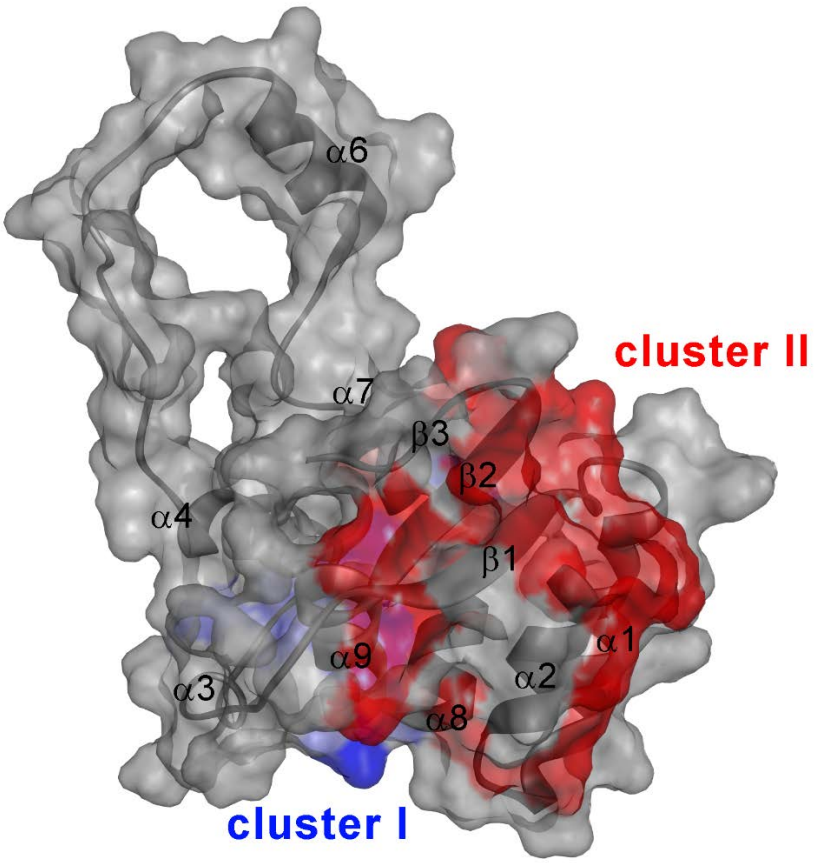

Figure S18. Surface and ribbon representation of hpTEN colored according the effects observed in ^{15}N-^{1}H HSQC spectra recorded in titration experiment of protein by fork **E8**. First group of signals (colored red) undergo slow exchange between free protein and its complex with **E8** (backbone amide resonances of the residues R2, F3, D4, D8, K11, R33, E34, W36, I37, R39, V40, K105, F109, R110, L122, S129, R131, G133, N134, V135 and side-chain resonances of the residues Q5 (Hε) and N10 (Hδ)). Upon the increase of concentration of **E8** signals that undergo fast exchange (colored blue) are also observed (backbone amide resonances of the residues Y54, S55, H56, S106, H113, I115, I116 and G117). These two groups of residues represent clusters II and I, respectively. Orientation of the protein is similar to that used in the figures 2 and 3.

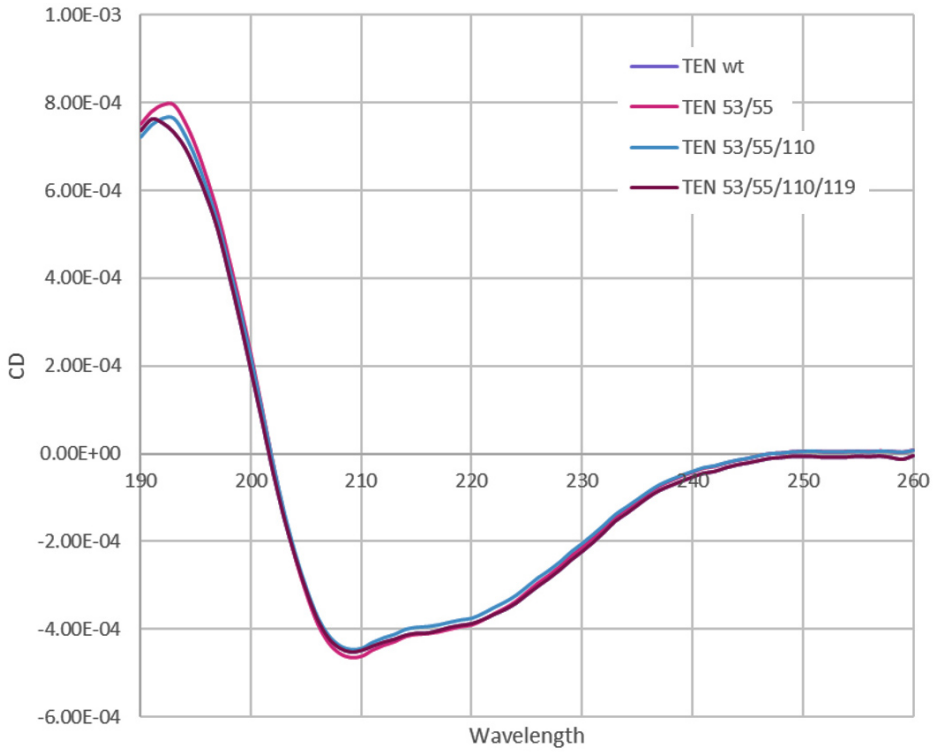

Figure S19. Circular dichroism spectra of the wild type hpTEN (lilac), hpTEN N53A/S55A (pink), hpTEN N53A/S55A/R110A (blue) and hpTEN N53A/S55A/R110A/E119A (purple).

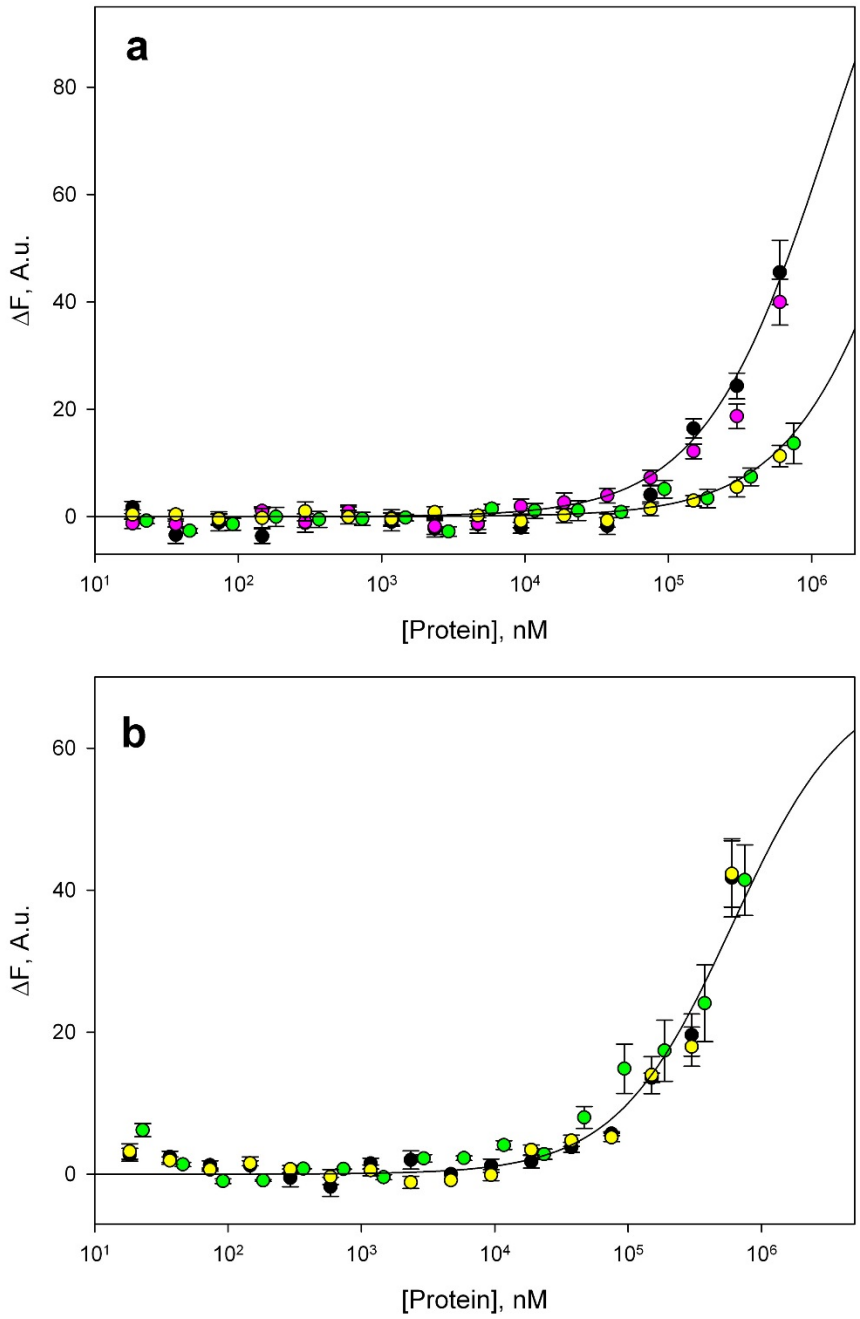

Figure S20. Results of thermophoresis titration of FAM-labeled oligonucleotides. (**a**) Titration of heteroduplex **E4** with the wild-type hpTEN (black circles) and its mutant variants: double N53A/S55A (pink), triple N53A/S55A/R110A (green), and 4-residue N53A/S55A/R110A/E119A (yellow). The value of K_d for double mutant variant is 1.3 mM, for triple and 4-residue variants 6.0 mM. ΔF=140 A.u. (**b**) Titration of FAM-labeled fork **E8** with the wild-type hpTEN (black circles) and its mutant variants: triple N53A/S55A/R110A (green), and 4-residue N53A/S55A/R110A/E119A (yellow). The titration curve is drawn for K_d = 0.3 mM and ΔF=70 A.u.

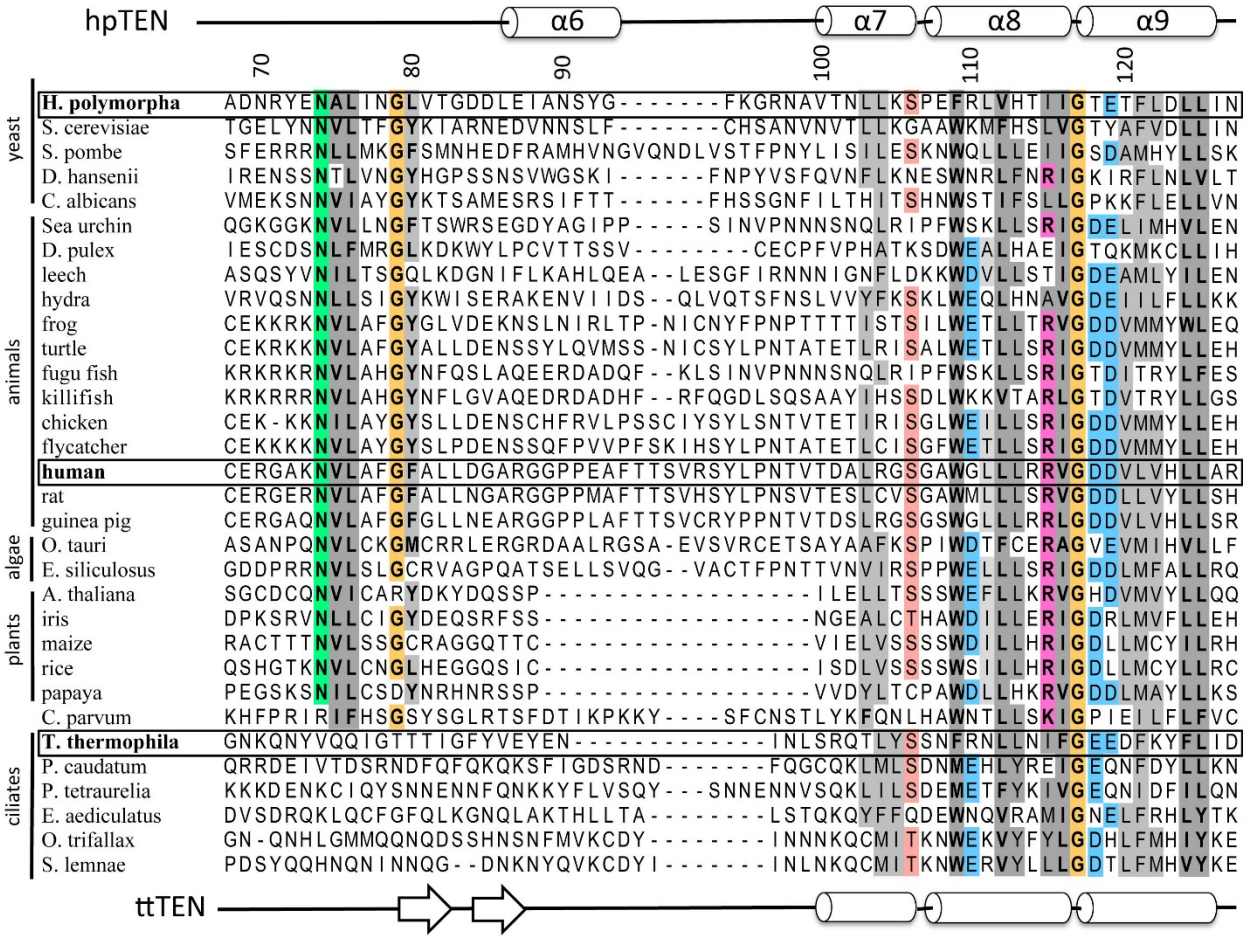

Figure S21. An alignment of a part of the TEN domain sequences from different organisms. The secondary structural elements shown above the table correspond to hpTEN, while those below the table to ttTEN. The conserved residues are colored as follows: hydrophobic in gray, glycine in orange, asparagine in green, serine or threonine in pink; arginine or lysine in magenta and aspartate or glutamate in blue. The sequence identifiers used in the alignment are listed in Online Methods.

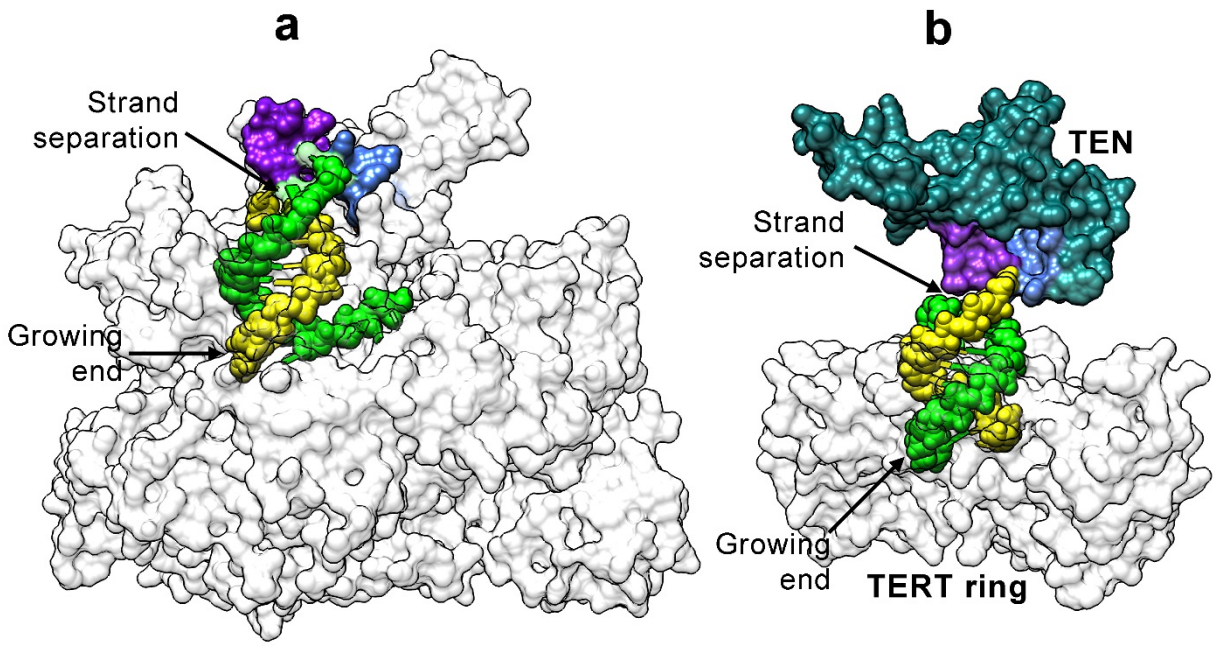

Figure S22. DNA/RNA heteroduplex bound to RNA polymerase II and TERT. (**a**) The structure of RNA polymerase II complexed with RNA product and DNA template (PDB ID code 1SFO (15)). The protein is shown as a light-gray surface; protein loops responsible for the strand separation in a heteroduplex are in purple ('lid') and blue ('rudder'). RNA strand of a duplex is in yellow, DNA strand in green. (**b**) The model of hpTERT complexed with DNA product and RNA template. The hpTERT ring in a predicted orientation to hpTEN is shown as a light-gray surface; hpTEN is shown as a dark cyan surface; the structural elements of hpTEN corresponding to the 'lid' and 'rudder' analogs are shown in purple and blue. RNA strand of the duplex is in yellow, DNA strand in green.

References to Supplementary Information

1. Krissinel, E. (2012) Enhanced fold recognition using efficient short fragment clustering. *J Mol. Biochem.*, **1**, 76-85.
2. Robert, X. and Gouet, P. (2014) Deciphering key features in protein structures with the new ENDscript server. *Nucleic Acids Res*, **42**, W320-W324.
3. Sievers, F., Wilm, A., Dineen, D., Gibson, T.J., Karplus, K., Li, W., Lopez, R., McWilliam, H., Remmert, M., Söding, J. *et al.* (2011) Fast, scalable generation of high-quality protein multiple sequence alignments using Clustal Omega. *Molecular Systems Biology*, **7**.
4. Boutet, E., Lieberherr, D., Tognolli, M., Schneider, M., Bansal, P., Bridge, A.J., Poux, S., Bougueleret, L. and Xenarios, I. (2016) In Edwards, D. (ed.), *Plant Bioinformatics: Methods and Protocols*. Springer New York, New York, NY, pp. 23-54.
5. Yang, J., Yan, R., Roy, A., Xu, D., Poisson, J. and Zhang, Y. (2015) The I-TASSER Suite: protein structure and function prediction. *Nat Meth*, **12**, 7-8.
6. Gillis, A.J., Schuller, A.P. and Skordalakes, E. (2008) Structure of the Tribolium castaneum telomerase catalytic subunit TERT. *Nature*, **455**, 633-637.
7. Mitchell, M., Gillis, A., Futahashi, M., Fujiwara, H. and Skordalakes, E. (2010) Structural basis for telomerase catalytic subunit TERT binding to RNA template and telomeric DNA. *Nature structural & molecular biology*, **17**, 513-518.
8. Bryan, C., Rice, C., Hoffman, H., Harkisheimer, M., Sweeney, M. and Skordalakes, E. (2015) Structural Basis of Telomerase Inhibition by the Highly Specific BIBR1532. *Structure*, **23**, 1934-1942.
9. Jacobs, S.A., Podell, E.R. and Cech, T.R. (2006) Crystal structure of the essential N-terminal domain of telomerase reverse transcriptase. *Nature structural & molecular biology*, **13**, 218-225.
10. Pettersen, E.F., Goddard, T.D., Huang, C.C., Couch, G.S., Greenblatt, D.M., Meng, E.C. and Ferrin, T.E. (2004) UCSF Chimera—A visualization system for exploratory research and analysis. *Journal of Computational Chemistry*, **25**, 1605-1612.
11. Popenda, M., Szachniuk, M., Antczak, M., Purzycka, K.J., Lukasiak, P., Bartol, N., Blazewicz, J. and Adamiak, R.W. (2012) Automated 3D structure composition for large RNAs. *Nucleic Acids Res*, **40**, e112-e112.
12. Emsley, P., Lohkamp, B., Scott, W.G. and Cowtan, K. (2010) Features and development of Coot. *Acta Crystallographica Section D*, **66**, 486-501.
13. Laskowski, R.A., MacArthur, M.W., Moss, D.S. and Thornton, J.M. (1993) PROCHECK: a program to check the stereochemical quality of protein structures. *Journal of Applied Crystallography*, **26**, 283-291.
14. Vriend, G. (1990) WHAT IF: A molecular modeling and drug design program. *Journal of Molecular Graphics*, **8**, 52-56.
15. Westover, K.D., Bushnell, D.A. and Kornberg, R.D. (2004) Structural basis of transcription: Separation of RNA from DNA by RNA polymerase II. *Science*, **303**, 1014-1016.